Supporting Information for

Alloying Two-Dimensional NbSi2N4: A New Strategy to Realize Half-Metallic Antiferromagnets

Yanxia Wang, Qinxi Liu, Xue Jiang*, Yi Wang, and Jijun Zhao

Key Laboratory of Material Modification by Laser, Ion and Electron Beams, Dalian University of Technology, Ministry of Education, Dalian 116024, China

Table S1. Bader analysis of $Nb_{1-x}Mn_xSi_2N_4$ (x = 0, 1/6, 1/4, 2/3, and 1). Δ(Nb), Δ(Mn), Δ(N1), Δ(N2), and Δ(Si) are the changes in charge of Nb, Mn, N1 (close to Mn), N2 (far from Mn), and Si atoms, respectively. Positive and negative values denote gain and loss of charge, respectively.

	Δ (Nb)	Δ (Mn)	Δ (N1)	Δ (N2)	Δ (Si)
$NbSi_2N_4$	−2.01	–	1.76	2.21	−2.97
$Nb_{5/6}Mn_{1/6}Si_2N_4$	−2.06	−1.12	1.70	2.22	−2.97
$Nb_{3/4}Mn_{1/4}Si_2N_4$	−2.10	−1.16	1.64	2.22	−2.97
$Nb_{1/3}Mn_{2/3}Si_2N_4$	−2.32	−1.38	1.59	2.22	−2.97
$MnSi_2N_4$	–	−1.45	1.47	2.21	−2.97

Table S2. Bond lengths (d) and bond angles (θ) for different TM atoms and N atoms and the vertical distances (d^v) between layers of Nb/Mn and N atoms of $Nb_{1-x}Mn_xSi_2N_4$ (x = 0, 1/6, 1/4, 2/3, and 1) monolayer structures.

	d_{TM-TM} (Å)			d_{TM-N} (Å)		d^v_{TM-N} (Å)		$\theta_{TM-N-TM}$
	Nb-Nb	Nb-Mn	Mn-Mn	Nb-N	Mn-N	Nb-N	Mn-N	
$NbSi_2N_4$	2.96	–	–	2.13	–	1.27	–	88.24
$Nb_{5/6}Mn_{1/6}Si_2N_4$	2.88/2.92	2.86	5.88	2.09	2.10	1.24	1.24	87.97
$Nb_{3/4}Mn_{1/4}Si_2N_4$	2.89/2.98	2.93	5.86	2.10	2.07	1.22	1.22	89.30
$Nb_{1/3}Mn_{2/3}Si_2N_4$	2.97	3.03	2.92	2.09	2.05	1.20	1.19	90.67
$MnSi_2N_4$	–	–	2.89	–	2.04	–	1.16	90.60

Table S3. The magnetic moments and magnetic ground states (GS) of $Nb_{1-x}Mn_xSi_2N_4$ (x = 0, 1/6, 1/4, 2/3, and 1) systems.

	M_{Nb} (μ_B)	M_{Mn} (μ_B)	M_{Total} (μ_B)	GS
$NbSi_2N_4$	0.9	–	0.9	FM
$Nb_{5/6}Mn_{1/6}Si_2N_4$	0.8, 0.2	–1.7	0.6	FIM
$Nb_{3/4}Mn_{1/4}Si_2N_4$	0.7	−2.2	0	AFM
$Nb_{1/3}Mn_{2/3}Si_2N_4$	0	3.0, −3.0	0	AFM
$MnSi_2N_4$	–	3.2, −3.2	0	AFM

Table S4. The possible interaction paths contain in $Nb_{1-x}Mn_xSi_2N_4$ and the corresponding magnetic ground state (GS).

	Nb-Nb	Nb-Mn	90º Nb-N-Mn	Mn-Mn	90º Mn-N-Mn	GS
$NbSi_2N_4$	☼	–	–	–	–	FM
$Nb_{5/6}Mn_{1/6}Si_2N_4$	☼	☼	☼	–	–	FIM
$Nb_{3/4}Mn_{1/4}Si_2N_4$	☼	☼	☼	–	–	AFM
$Nb_{1/3}Mn_{2/3}Si_2N_4$	–	–	–	☼	☼	AFM
$MnSi_2N_4$	–	–	–	☼	☼	AFM

Table S5. Energy (eV) of different magnetic configurations of $V_{3/4}Mn_{1/4}Si_2N_4$, $Nb_{2/3}Fe_{1/3}Si_2N_4$, $V_{2/3}Fe_{1/3}Si_2N_4$, $Nb_{1/2}Co_{1/2}Si_2N_4$ and $V_{1/2}Co_{1/2}Si_2N_4$.

	$V_{3/4}Mn_{1/4}Si_2N_4$	$Nb_{2/3}Fe_{1/3}Si_2N_4$	$V_{2/3}Fe_{1/3}Si_2N_4$	$Nb_{1/2}Co_{1/2}Si_2N_4$	$V_{1/2}Co_{1/2}Si_2N_4$
FM	–224.015	–344.989	–331.112	–223.124	–215.960
AFM1	**–224.497**	**–345.148**	**–331.771**	**–223.388**	**-215.962**
AFM2	–224.197	–344.862	–331.365	–223.386	-215.961
AFM3	–224.035	–345.134	–331.393	–	–

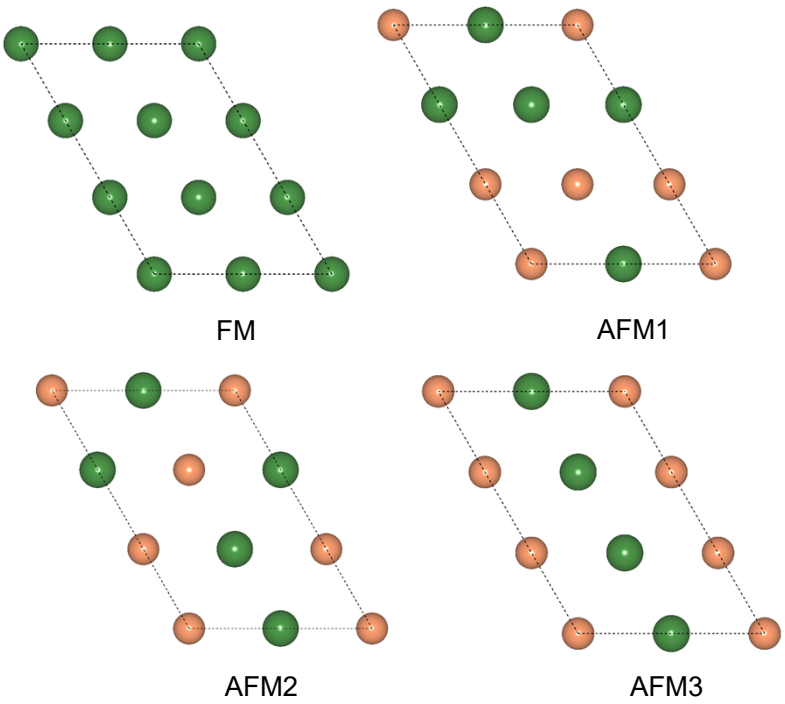

Fig. S1. 2 × 3 supercells of $NbSi_2N_4$ monolayer in FM and AFM magnetic configurations. Green and orange balls represent Nb atoms in spin-up and spin-down states, respectively. The Si and N atoms are omitted for simplicity.

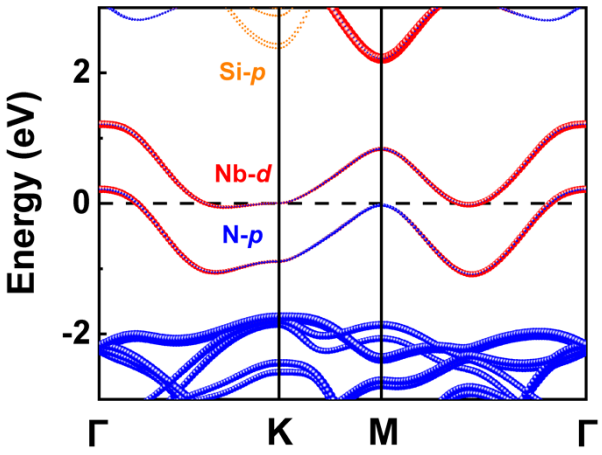

Fig. S2. Atom-projected band structure for monolayer $NbSi_2N_4$. The scale indicates the magnitude of the projection.

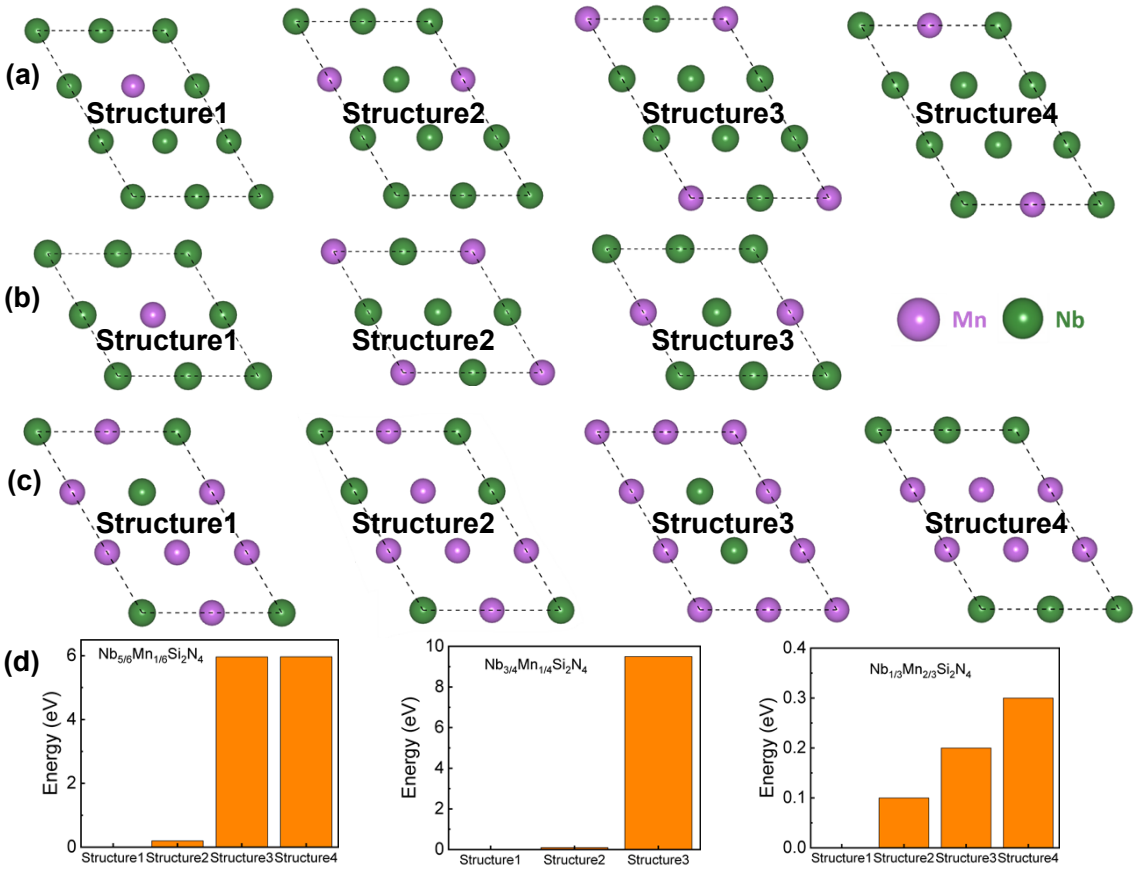

Fig. S3. Considered possible distribution structures of Nb and Mn atoms in a 2 × 3 or 2 × 2 supercell for (a) $Nb_{5/6}Mn_{1/6}Si_2N_4$, (b) $Nb_{3/4}Mn_{1/4}Si_2N_4$, and (c) $Nb_{1/3}Mn_{2/3}Si_2N_4$. Purple and green balls represent Mn and Nb atoms, respectively. The Si and N atoms are omitted for simplicity. (d) Relative energies per supercell for each considered structure of $Nb_{5/6}Mn_{1/6}Si_2N_4$, $Nb_{3/4}Mn_{1/4}Si_2N_4$, and $Nb_{1/3}Mn_{2/3}Si_2N_4$.

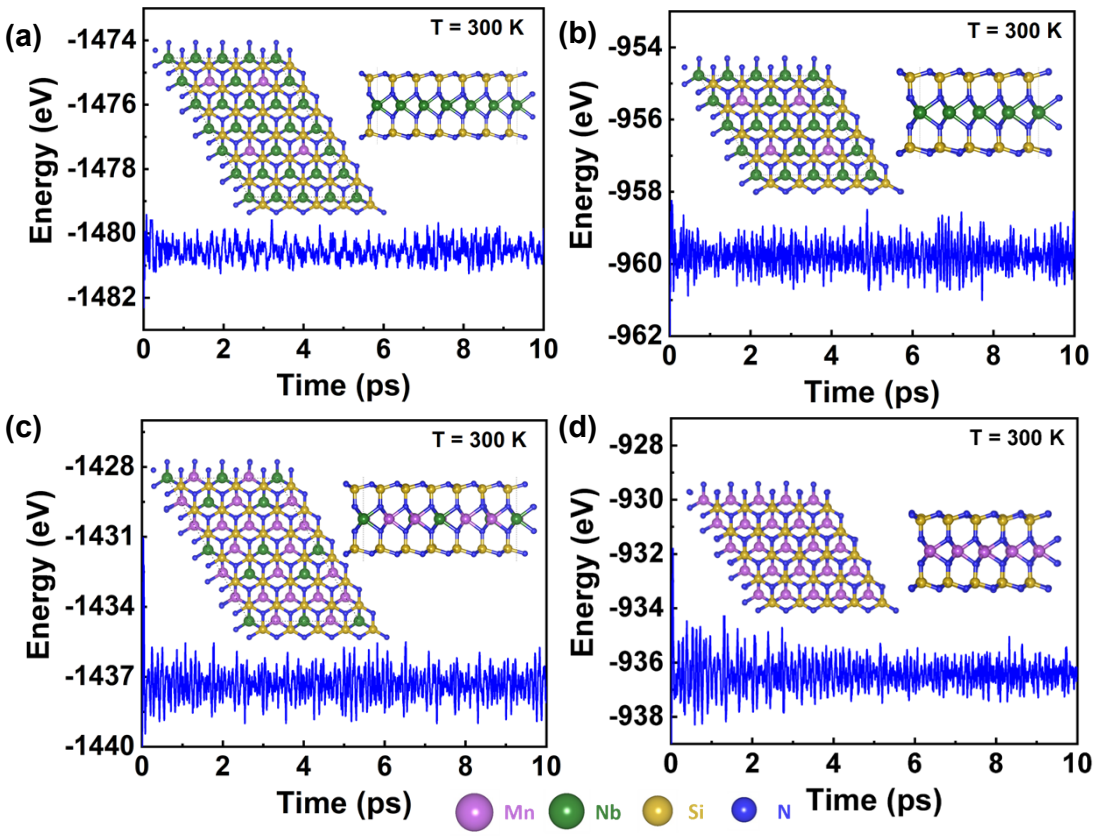

Fig. S4. Total energy fluctuation of 4 × 4 × 1 supercell for (a) $Nb_{3/4}Mn_{1/4}Si_2N_4$ and (d) $MnSi_2N_4$ monolayers and 4 × 6 × 1 supercell for (b) $Nb_{5/6}Mn_{1/6}Si_2N_4$ (c) $Nb_{1/3}Mn_{2/3}Si_2N_4$ monolayer during AIMD simulation for 10 ps at 300 K. The insets show the top and side views of the geometries at the end of 10 ps simulation.

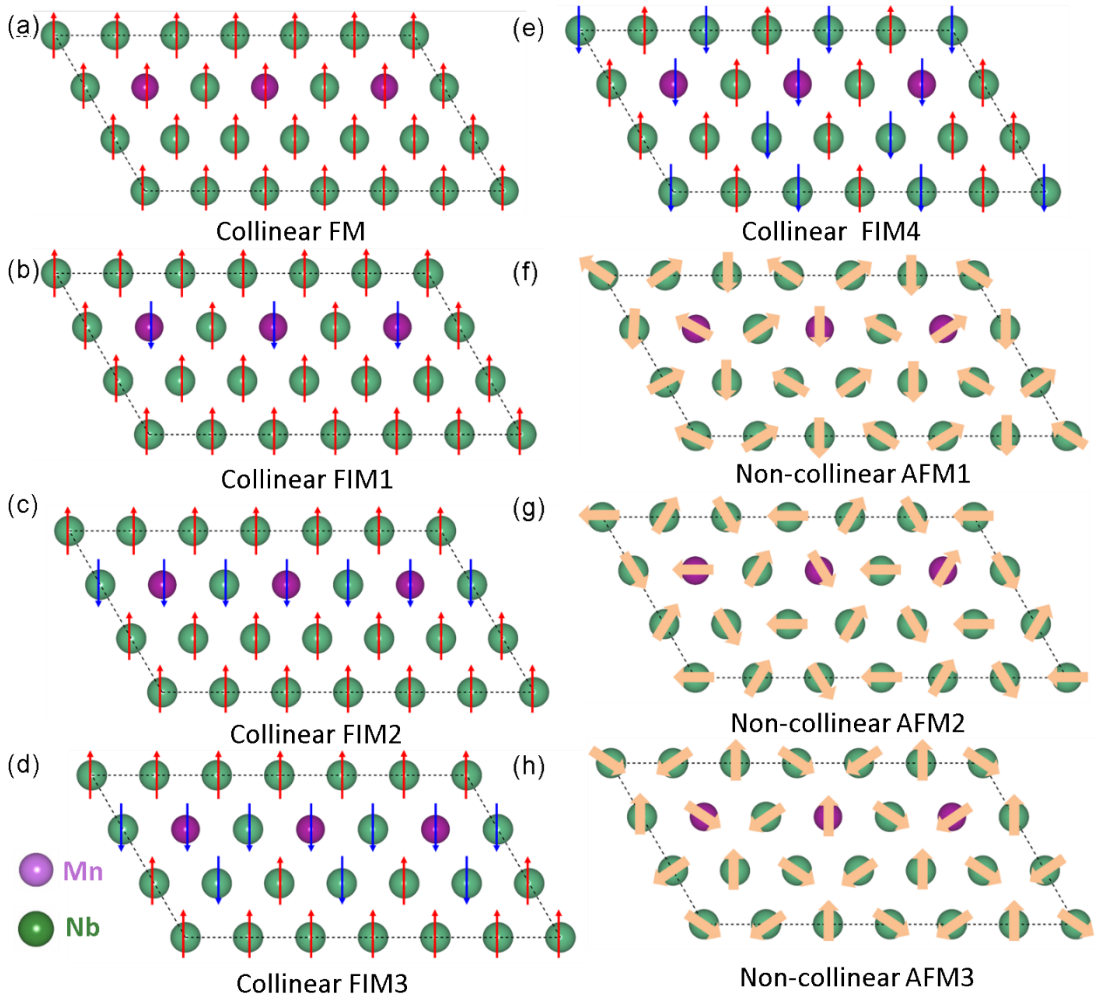

Fig. S5. Schematic plots of $Nb_{5/6}Mn_{1/6}Si_2N_4$ monolayers in different (a) collinear ferromagnetic (FM), (b-e) collinear ferrimagnetic (FIM), and (f-h) 120° non-collinear antiferromagnetic (AFM) states in a 3 × 6 supercell. Green and purple balls represent Nb and Mn atoms, respectively. The Si and N atoms are omitted for simplicity. Red and blue arrows represent collinear spin-up and spin-down states, respectively. Orange arrows represent in-plane non-collinear spin states.

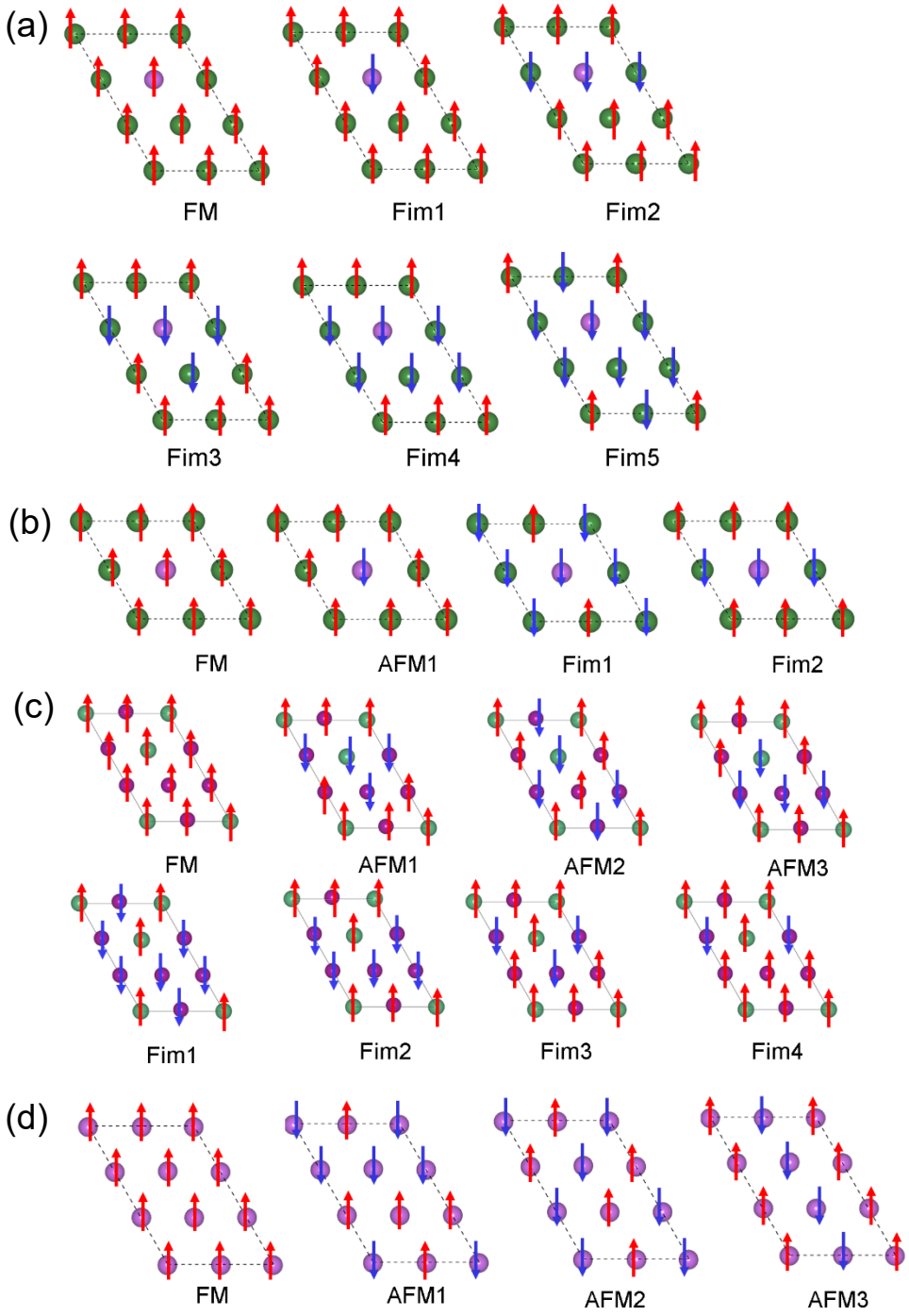

Fig. S6. Schematic plots of (a) $Nb_{5/6}Mn_{1/6}Si_2N_4$, (b) $Nb_{3/4}Mn_{1/4}Si_2N_4$, (c) $Nb_{1/3}Mn_{2/3}Si_2N_4$, and (d) $MnSi_2N_4$ monolayers in different ferromagnetic (FM), ferrimagnetic (Fim), and antiferromagnetic (AFM) states in a 2 × 3 or 2 × 2 supercell. Green and purple balls represent Nb and Mn atoms, respectively. Red and blue arrows represent spin-up and spin-down states, respectively.

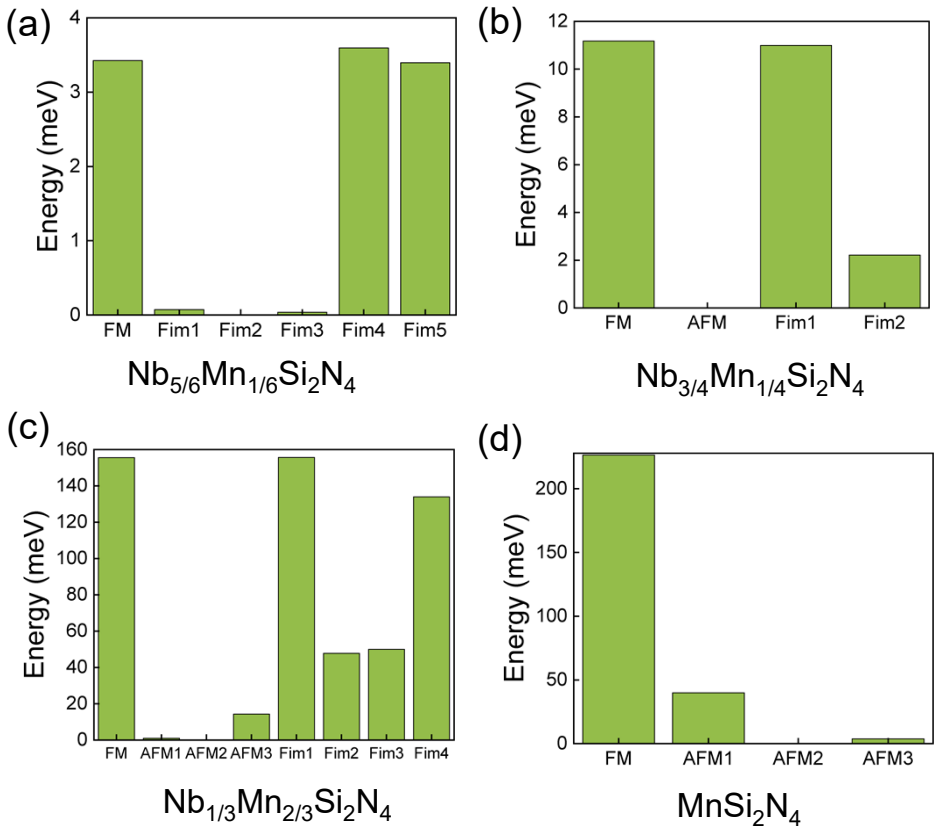

Fig. S7. Relative energies per formula unit cell for each considered magnetic structure of (a) $Nb_{5/6}Mn_{1/6}Si_2N_4$, (b) $Nb_{3/4}Mn_{1/4}Si_2N_4$, (c) $Nb_{1/3}Mn_{2/3}Si_2N_4$, and (d) $MnSi_2N_4$.

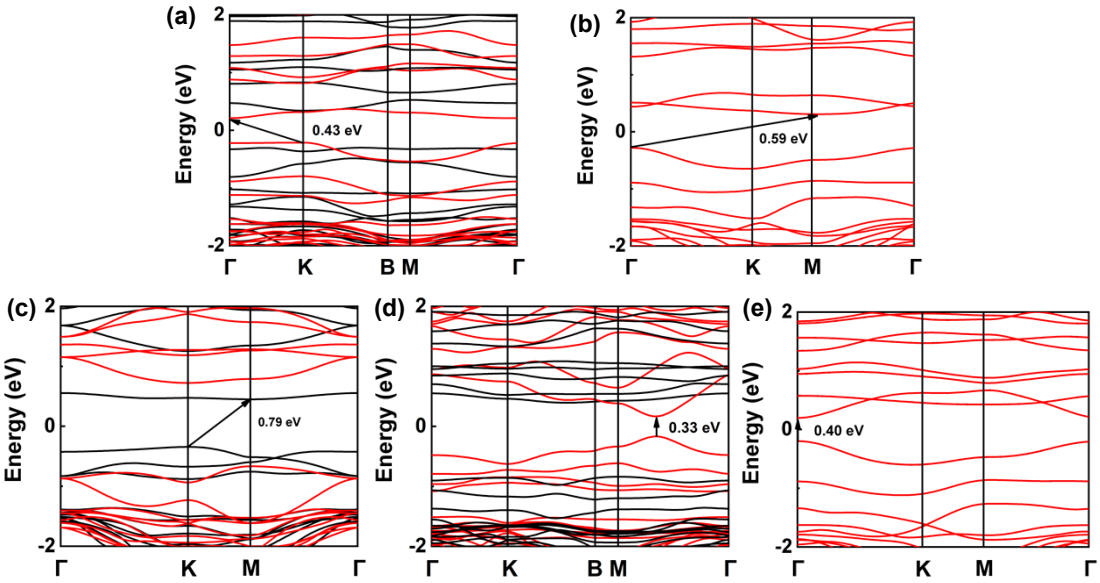

Fig. S8. Band structures of (a) $Nb_{2/3}Fe_{1/3}Si_2N_4$, (b) $Nb_{1/2}Co_{1/2}Si_2N_4$, (c) $V_{3/4}Mn_{1/4}Si_2N_4$, (d) $V_{2/3}Fe_{1/3}Si_2N_4$, and (e) $V_{1/2}Co_{1/2}Si_2N_4$. Black and red color lines represent spin-up and spin-down states, respectively.